



## Research article

# Dynamics of soil organic carbon and nitrogen and their relations to hydrothermal variability in dryland

Mingzhu He <sup>a,\*</sup>, Liang Tang <sup>a,1,\*</sup>, Chengyi Li <sup>a,b</sup>, Jianxin Ren <sup>c</sup>, Libin Zhang <sup>a,b</sup>, Xinrong Li <sup>a</sup>

<sup>a</sup> Shapotou Desert Research and Experiment Station, Northwest Institute of Eco-Environment and Resources, Chinese Academy of Sciences, 730000, Lanzhou, Gansu, China

<sup>b</sup> University of Chinese Academy of Sciences, 100000, Beijing, China

<sup>c</sup> Hami Agricultural Product Quality and Safety Inspection and Testing Center, 839000, Hami, Xinjiang, China



## ARTICLE INFO

## Keywords:

Soil organic carbon  
Soil total nitrogen  
Climate change  
Machine learning  
Structural equation model

## ABSTRACT

Carbon (C) and nitrogen (N) cycles of terrestrial ecosystems play key roles in global climate change and ecosystem sustainability. In recent decades, climate change has threatened the nutrient balance of dryland ecosystems. However, its impact on soil organic carbon (SOC) and soil total nitrogen (STN) in drylands of China are still unclear. In this study, the structural equation model (SEM) was used to explain the relationship between environmental variables used by the best model and SOC or STN. Then Adaptive Boosting Regressor (AdaBoost), Gradient Boosting Regression (GBRT), Extreme gradient boosting Regression (XGBoost) and Random Forest Regression (RF) were used to establish the prediction model of SOC and STN based on soil samples along with environmental variables. The performance of these models was assessed based on a 10-fold cross-validation method using three statistical indicators. Finally, we predicted the SOC and STN of soil samples from 2000 to 2019 based on the best model. Overall, the RF model performed better at predicting SOC and STN in drylands than the other three prediction models (AdaBoost, GBRT, XGBoost). Climate factors were the main factors affecting SOC and STN in the study area. In the Alashan, a dryland in northern China, the precipitation in the growing season increased from 2000 to 2019, at a rate of 12.9 mm/decade. During the same period, the annual sunshine duration significantly decreased by 66 h/decade. Along with interannual hydrothermal variability, SOC showed a fluctuating upward trend at a rate of 0.04 g/kg/decade, while STN exhibited a fluctuating downward trend at 0.003 g/kg/decade from 2000 to 2019. Due to the effects of climate change, dryland were considered as potential sites for carbon sequestration. However, due to the annual hydrothermal variance causing dynamic annual changes, it was deemed unstable. Moreover, it would cause STN loss, which might reduce soil fertility. More attention should be paid to STN monitoring in dryland in the future.

## 1. Introduction

Carbon (C) and nitrogen (N) cycles of terrestrial ecosystems play key roles in global climate change and ecosystem sustainability (Zeraatpisheh et al., 2019). Due to the impact of climate change, most regions in the world are experiencing increasingly severe drought, which is mainly characterised by a decrease in regional precipitation and an increase in evapotranspiration (Liu and Chen, 2021). However, these changes may decrease plant photosynthesis and premature senescence and reduce the input of soil C and N (Holz et al., 2018). This will also change the composition of soil microorganisms and enzyme activities, thus affecting the balance of soil C and N (Ren et al., 2017), accelerating

soil C loss (Mikha et al., 2005), and inhibiting soil N mineralisation (Hartmann et al., 2013). Due to climate change, predicting spatial and temporal characteristics of SOC and STN is crucial for maintaining food security and improving environmental quality (Gholizadeh et al., 2018). Generally, traditional investigation methods for SOC and STN mainly rely on ground investigation and laboratory analysis (Forkuor et al., 2017), which is resource-intensive. Therefore, this study aimed to find an efficient, fast, and accurate method to predict the spatial variation of SOC and STN in unvisited locations or areas with rare fixed-point soil data.

The soil-landscape model, which assumed that soil development is determined by climate, biology, topography, parent material, and time,

\* Corresponding author.

E-mail addresses: [hmzecology@lzb.ac.cn](mailto:hmzecology@lzb.ac.cn) (M. He), [tangliangdyx@163.com](mailto:tangliangdyx@163.com) (L. Tang).

<sup>1</sup> These authors contributed equally to this work and should be considered co-first authors.

was first proposed by V.V. Dokuchaev and then formulated by Jenny (Guo et al., 2016; Leiningen, 1931). Through soil-landscape modeling, SOC and STN can be well predicted by environmental variables (Leiningen, 1931). At present, the development of remote sensing and computer technology has created more means to obtain environmental variables (terrain parameters: DEM; vegetation or soil information: Landsat, MODIS, SPOT etc.; Meteorological: Climatic Research Unite, European Climate Assessment&Dataset, WorldClim, etc.) (Kalambukattu et al., 2018), and the accuracy of new prediction models (Random Forest (RS), Support Vector Machines (SVM), Boosted Regression Trees (BoRT)) is increasing (Khanal et al., 2018; Zeraatpisheh et al., 2019; Zhou et al., 2020). Indeed, the soil-landscape model has good prediction accuracy for areas with strong spatial heterogeneity of soil types or soil attributes, such as mountain areas (Zhu et al., 2010), and poor in the low-lying areas such as plains and farmlands with weak heterogeneity of altitude, slope, and vegetation (Iqbal et al., 2005). At present, soil-landscape models which are suitable for high biomass areas such as forests, grasslands, and farmland have been established (Shahhosseini et al., 2019; Tajik et al., 2020). However, a more accurate prediction model for SOC or STN based on soil-landscape models is lacking in dryland areas. In addition, previous scholars used the soil-landscape models to reveal the spatial distribution characteristics of soil properties in the study area (Zeraatpisheh et al., 2019; Khanal et al., 2018) but failed to reveal the relationship between soil properties and environmental variables, and the impact of changes in environmental variables on soil properties, especially in dryland.

Drylands account for about 41% of global terrestrial land surfaces and are home to 2.5 billion people (Grace et al., 2006). Due to the low soil fertility of dryland, these areas are exceedingly sensitive to degradation caused by climate change (Li et al., 2016). In the last 100 years, the greatest warming occurred in drylands (Huang et al., 2017). The region of northwest and Inner Mongolia is the main dryland in China; characterised by a dry climate, minimal rainfall, and a fragile ecological environment (Wieder et al., 2015). Due to the influence of climate change in the past decades, dryland ecosystems in Northwest China are in disequilibrium (Reynolds et al., 2007). The temperature in the

dryland of northwest China shows a significant upward trend, and the precipitation has increased with a trend of 3.2mm/decade (Li et al., 2012). However, the change of SOC and STN in soil are sensitive to climate change (Fang et al., 2019). Climate change can affect carbon storage by affecting the environmental conditions of carbon mineralisation (Bontti et al., 2009) and plant growth (Bai et al., 2010). C and N cycles in terrestrial ecosystems are two closely related processes. The storage of C in ecosystems is affected by the availability of N (Luo et al., 2009). In recent decades, climate change has threatened the balance of dryland ecosystems, but the impact of climate change on SOC and STN in arid areas of China is still unclear.

Therefore, the purposes of this study are 1) to filter the environmental variables affecting SOC and STN in dryland areas; 2) to establish an accurate prediction model of SOC and STN in arid areas of China with the data of environmental variables (climate, topography, soil, and vegetation), according to the idea of soil-landscape model; 3) to reveal the relationship between environmental variables and SOC or STN; and 4) to enhance the understanding of the characteristic variation of SOC and STN in the context of climate change in dryland.

## 2. Materials and methods

### 2.1. Study area and soil data

The study area is located in the eastern wing of the desert in central Asia and belongs to the Alashan League of Inner Mongolia Autonomous Region, China (Fig. 1). This area is dominated by deserts and desertification land, accounting for approximately 29% of the total area. Affected by an extremely arid climate, vegetation in this area shows a sparse distribution (Yuan et al., 2018). This area is characterised by low precipitation, higher evaporation, strong winds, extreme temperature differences between day and night, hot summers, and cold winters. The topography of Alashan shows that the south is higher than the north, with widely distributed deserts. Alashan has a fragile ecological environment and is one of the birthplaces of sandstorms in China.

In September 2019, 70 soil samples were collected from the Alashan

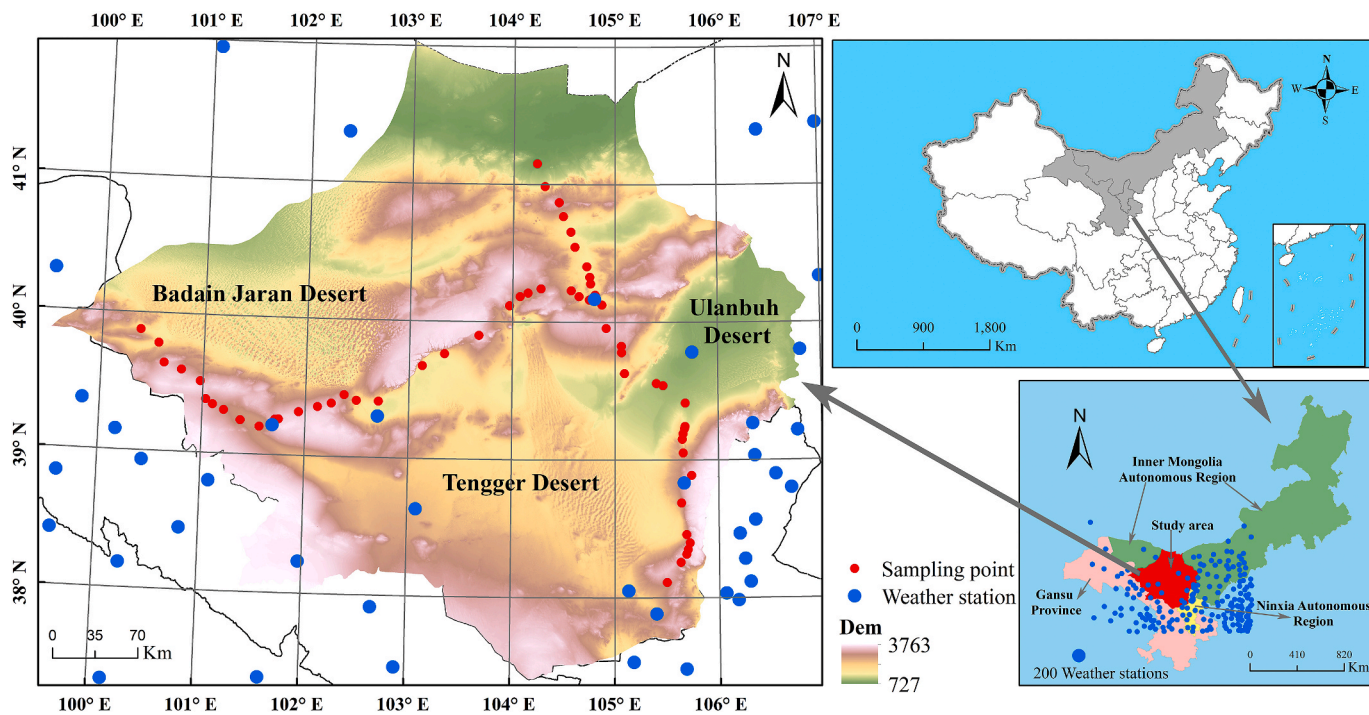


Fig. 1. Spatial distribution of sampling points and weather stations. Red dots are sampling points, and blue dots are weather stations. The 200 weather stations in the traction map in the lower right corner were used to interpolate the regional meteorological data by ANUSPLIN interpolation. (For interpretation of the references to colour in this figure legend, the reader is referred to the Web version of this article.)

(Fig. 1), including topsoil samples (0–5 cm). In order to reduce the impact of human activities, samples were mainly located in the area covered by the natural vegetation that is less affected by human activities such as grazing and fertilisation. The Tengger Desert, Badain Jaran Desert, and Ulanbuh Desert were distributed in a triangular shape to make up the study area. Most of this area is covered with sand, with sparse vegetation growing on the edge of the desert; thus, sampling points are distributed in the desert border area. In addition, the sampling did not have great coverage because some areas were inaccessible. The amount of SOC was determined by means of wet oxidation with dichromate (Walkley and Black, 1934). STN was measured by a Kjeltec System 2300 (Foss Inc., Hillerød, Denmark).

## 2.2. Environmental variables

Forty-eight environmental variable data sets were selected to predict the content of SOC and STN. Nine topographic attributes were obtained from a Digital Elevation Model (DEM) ([www.gscloud.cn/](http://www.gscloud.cn/)): Elevation, Slope, Aspect, Roughness, Relief Amplitude, Slope of Aspect, Stream Power Index, Sediment Transport Index, and Topographic Wetness Index. The spatial distribution map of meteorological elements in the study area was obtained by ANUSPLIN interpolation based on 200 weather stations in and around the study area (Fig. 1). Climate data from 2000 to 2019 were obtained, including annual and seasonal mean temperatures, annual and seasonal accumulated temperatures, annual and seasonal mean surface temperatures, annual and seasonal cumulative precipitation, cumulative precipitation in the growing season (June to October), annual and seasonal mean relative humidity, and annual and seasonal sunshine duration. Meteorological station data were obtained through the Data Center of Resources and Environmental Sciences, Chinese Academy of Sciences. The normalised difference vegetation index (NDVI) and enhanced vegetation index (EVI) from 2000 to 2019 were derived from the Terra Moderate Resolution Imaging Spectro-radiometer (MODIS) 16-day composite products, with a spatial resolution of 250m. The data were acquired from the NASA ftp website (<ftp://e4ft101u.ecs.nasa.gov/MOLT/>).

## 2.3. Structural equation model

Structural equation model (SEM) was developed from the concept of path analysis proposed by Sewll Wright in the 1920s, and is a statistical method proposed by Karl. Joreskog in the 1970s to analyse the relationship between variables based on the covariance matrix (Ullman, 2001; Wright, 1934). Its most prominent characteristic is that it applies the concept of a latent variable to the model and integrates path analysis, confirmatory factor analysis, and general statistical test methods to analyse the causal relationship between variables (Tankak, 1990). The SEM also considers error factors, makes up for the shortcomings of factor analysis, is not limited by the hypothetical conditions of path analysis, and allows certain errors between independent variables and dependent variables (Grace and Keeley, 2006).

## 2.4. Machine learning algorithm

### 2.4.1. Adaptive Boosting Regressor

Adaptive Boost (AdaBoost) is an iterative algorithm in ensemble learning. Its core purpose is to train different classifiers (weak classifiers) for the same training set and then assemble these weak classifiers into a stronger final regression (strong regression) (Avnimelech and Intrator, 1999). The weight of each sample is determined according to the classification correctness of each sample in each training set and the last overall classification (Friedman, 2001). The new data with modified weights are sent to the lower-level regressions for training, and finally, the regressions obtained every time are coalesced into the final decision regression (Seo et al., 2017).

### 2.4.2. Gradient boosting regression

Gradient boosting can also be called a multi-layered decision tree. The algorithm was proposed by Friedman at the beginning of the 20th century and has a strong nonlinear fitting ability (Natekin and Knoll, 2013). The GBRT is composed of multiple decision trees; the final result is only necessary to add the output results of all decision trees. To prevent over-fitting, a boosting process is added (Albatineh, 2019). The original Boost algorithm will give each sample the same weight and then start training the model. If the model is heading in the right direction, it will reduce its weight; while if it is heading in the wrong direction, the weight will increase. After n iterations, the incorrect points will have the highest weights, and we get n simple classifiers, which can be combined to get the final model (Guo et al., 2016).

### 2.4.3. Extreme gradient boosting regression

Extreme gradient boosting regression (XGBoost) is a tree structure, which is an improvement of the gradient boosting regression algorithm optimised by the additive learning model (Friedman, 2001). Continuous iteration generates a new tree, and subtrees are added to make the model approach the sample distribution continuously. Finally, several tree models with low classification accuracy are combined into one model with high accuracy. Regularisation terms are added to XGboost loss function to control the complexity, reduce variance, and avoid over-fitting. The loss function optimisation of GBRT is the first derivative, XGBoost is expanded by the second Taylor expansion, allowing the first and second derivatives to be used simultaneously (Chen and Guestrin, 2016).

### 2.4.4. Random Forest Regression

Random forest (RF) is a classified regression model which contains multiple decision trees in which the output category is determined by the number of categories output by individual trees. RF contains many decision trees with high prediction accuracy, weak correlation or even irrelevance, forming a combination prediction model. After integration, many prediction models will jointly participate in predicting the values of the new observation output variables to obtain higher accuracy (Breiman, 2001). The RF model has the advantages of improving prediction accuracy, reducing overfitting, is insensitive to missing data and multivariate collinearity, and has the ability to deal with a large number of quantitative and qualitative data (Scornet et al., 2015).

## 2.5. Accuracy evaluation

We used four machine learning algorithms to predict SOC and STN and used 10-fold cross-validation with 100 replications to evaluate the predictive performance (Mahmoudzadeh et al., 2020). The whole dataset was randomly split into calibration (70%) and validation (30%) sets to model. In order to compare the model performance of the four prediction models above, three validation criteria were selected, including the root mean square error (RMSE), the mean absolute error (MAE), and the coefficient of determination ( $R^2$ ). These measures of model performance are described as follows (Wang et al., 2018b):

$$RMSE = \sqrt{\frac{1}{n} \sum_{i=1}^n (P_i - O_i)^2} \quad (1)$$

$$MAE = \frac{1}{n} \sum_{i=1}^n |P_i - O_i| \quad (2)$$

$$R^2 = \frac{\sum_{i=1}^n (P_i - \bar{O}_i)^2}{\sum_{i=1}^n (O_i - \bar{O}_i)^2} \quad (3)$$

where  $P_i$  is the predicted value,  $O_i$  is the true value, and n is the number of validated observations.

### 3. Results

#### 3.1. Descriptive analysis of SOC and STN

Descriptive analyses of SOC and STN in the study area are presented in Table 1. The median of SOC (2.25 g/kg) and STN (0.21 g/kg) were smaller than the average (SOC: 2.48 g/kg, STN: 0.25 g/kg), which indicated that half of the sample points were below the average, and contained great differences among them. The results showed that SOC and STN in most areas of the study area were lower than the average. While the range (SOC: 5.89 g/kg, STN: 0.89 g/kg) was dramatically higher than the average, the difference between the interquartile range and the mean or median was small; this indicated that there were areas with high or low SOC and STN in the research area, but the proportion was small. Variance and standard deviation were high, with a strong dispersion among the sampling points. Index values of degree of dispersion indicated that the differences in SOC and STN in different areas of the study area were significant. SOC and STN had right skewness, which could be evaluated from skewness and kurtosis, indicating that was more data on the left side of the mean. It also showed that SOC and STN in most areas of the study area were lower than the average. Overall, central tendency, degree of dispersion, and distributional pattern indicated that SOC and STN had strong spatial heterogeneity in the study area.

#### 3.2. Relationship between environmental variables and SOC or STN

In the study, 48 environmental variable data sets were selected to predict SOC and STN. The SEM was used to explain the relationship between them and was successfully fitted to our data at SOC and STN, satisfying the goodness-of-fit metrics (RMSEA<0.08, GFI>0.9, CFI>0.9, NFI>0.9, P > 0.05; Fig. 4). Together, 8 out of 48 variables explained 36% of the variations in SOC and 6 out of 48 variables explained 58% of the variations in STN.

As shown in Table 2 and Fig. 2, effects of environmental variables were classified into standardised direct, indirect, and total effects in the model. Indirect effect plus direct effect equalled total effect. EVI is a primary index in biophysical parameter products of remote sensing, which can reduce the disturbances of atmospheric and soil noise together and effectively respond to vegetation distribution in the measured area (Huete et al., 2002). SEM had shown that annual sunshine duration (SSD), mean relative humidity in spring (RHUSP), precipitation in the growing season (PREGS), silt particle content (SILT), relief amplitude (RA), roughness (RU), slope (SLO), and mean relative humidity in autumn (RHUAU) were the main factors influencing SOC changes. Moreover, PREGS and SILT exerted a direct effect on SOC, whereas other factors directly or indirectly affected vegetation (EVI), PREGS, and SILT, eventually changing SOC. In addition, effects of climatic factors (RHU (0.478), PREGS (0.398), and SSD (0.219)) on SOC were significantly stronger than topographic features (SLO (0.174), RU (0.161), and RA (0.120)) and soil texture (SILT (0.253)). PREGS, SILT directly affect STN, while Accumulated temperature in winter (ATEMWI), RU, RA directly or indirectly affect vegetation (EVI), PREGS,

**Table 1**  
Summary statistics of SOC and STN data.

Attributes		SOC	STN
Central tendency	Average (g/kg)	2.48	0.25
	Median (g/kg)	2.25	0.21
Degree of dispersion	Range (g/kg)	5.89	0.89
	Interquartile range (g/kg)	1.11	0.12
	Variance	2.17	0.04
	Standard deviation	1.46	0.2
	Coefficient of dispersion	0.59	0.8
Distributional pattern	Skewness	0.57	1.25
	Kurtosis	-0.4	1.31

**Table 2**

Standardised total, direct and indirect effects of environmental variables on SOC and STN analysed by structural equation modeling.

Environmental variables	SOC			STN		
	Total effects	Direct effects	Indirect effects	Total effects	Direct effects	Indirect effects
SSD	0.219	0	0.219	-	-	-
PREGS	0.398	0.308	0.090	0.587	0.326	0.261
SILT	0.253	0.189	0.064	0.458	0.265	0.194
RA	0.120	0	0.120	0.052	0	0.052
RU	0.161	0	0.161	0.076	0	0.076
SLO	0.174	0	0.174	-	-	-
RHU	0.478	0	0.478	-	-	-
EVI	0.231	0.231	0	0.347	0.347	0
ATEMWI	-	-	-	0.214	0	0.214

Notes: Direct effects are simple paths and are equal to the path coefficients in Fig. 4. Indirect effects are the sum of the products of the chain of path coefficients for all compound paths for which the independent variable is connected to the dependent variable while maintaining the causal direction of the arrows. Total effects are the sum of direct and indirect effects. The values indicate changes of SOC or STN per standardised-unit change of environmental variables.

SILT indirectly affected STN. Likewise, for STN alterations, climatic factors (PREGS (0.587) and ATEMWI (0.214)) had a higher impact than soil texture (SILT (0.458)) and topographic features (RU (0.076) and RA (0.052)).

#### 3.3. Performance of machine learning algorithms

We used SEM to reveal the relationship between environmental variables and SOC and STN, and found the main environmental factors that affect the change of SOC and STN. Based on the concept of the soil-landscape model, we used these environmental variables to establish the prediction model of SOC and STN. The prediction results of SOC and STN using four machine learning algorithms are presented in Figs. 3 and 4. Overall, RF had the highest prediction accuracy for SOC ( $R^2 = 0.71$ , RMSE = 0.94, MAE = 0.76) and STN ( $R^2 = 0.76$ , RMSE = 0.13, MAE = 0.10) (which accounts for 70.7% and 76.2% of the total variation of SOC and STN, respectively). Further, the prediction result of STN was better than SOC. Regarding the result of accuracy evaluation, the prediction performance hierarchy for SOC was as follows: RF > AdaBoost > GBRT > XGBoost. That of STN was RF > AdaBoost > XGBoost > GBRT.

The rankings of predictor variables for SOC and STN predicting using RF ordered by relative importance are shown in Figs. 3(D) and Fig.4(D), respectively. In the RF, 8 out of 48 variables could account for 70.7% ( $R^2_{SOC} = 70.7\%$ ) of the total variation of SOC (Fig. 3(E)). SSD, RHUSP, PREGS, SILT, RA, RU, SLO, and RHUAU were the most effective environmental variables in predicting SOC. Among them, SSD (38.5%), RHUSP (18.1%), PREGS (8.7%), and RHUAU (5.2%), representing climate variables, accounted for 70.5% of  $R^2_{SOC}$ . Furthermore, RU (8.7%), RA (7.6%), and SLO (5.4%), representing topographic features, accounted for 21.7% of  $R^2_{SOC}$ , while SILT, representing soil texture, accounted for 7.7% of  $R^2_{SOC}$ . In the RF, 5 out of 48 variables could account for 76.2% ( $R^2_{STN} = 76.2\%$ ) of the total variation of STN (Fig. 4(E)). PREGS, RU, SILT, ATEMWI, and RA were the most effective environmental variables in predicting STN. Among them, PREGS (45.3%) and ATEMWI (14.0%), representing climate variables, accounted for 59.3% of  $R^2_{STN}$ . RU (18.1%) and RA (7.0%), representing topographic features, accounted for 25.1% of  $R^2_{STN}$ , while SILT (15.6%), representing soil texture, accounted for 15.6% of  $R^2_{STN}$ . The above results showed that climate was the main driver for SOC and STN distribution in the arid desert area, followed by topography and soil texture.

#### 3.4. Changes in climatic elements of the study area from 2000 to 2019

The above analysis indicated that climatic variables were potentially

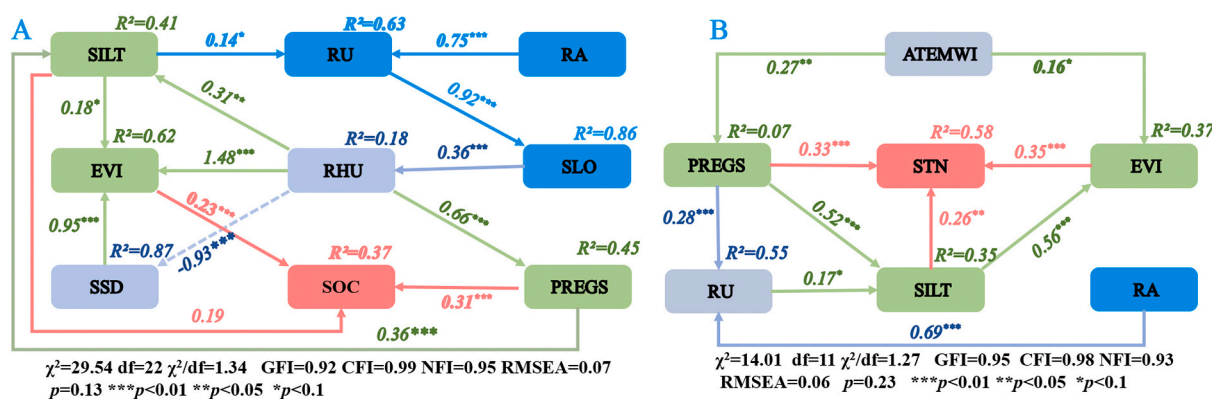


**Fig. 2.** Structural equation model relating environmental variables to SOC(A) or STN(B). Rectangles represent observed variables. A single arrow indicates the direct effect of a variable assumed to be a cause on another variable that is assumed to be an effect. Solid arrows denote positive relationships, while dashed arrows correspond to negative ones. Numbers in bold on arrows are standardised path coefficients. Percentages in italics on rectangles indicate the variance explained by the model ( $R^2$ ). SSD, annual sunshine duration; PREGS, precipitation in growing season; SILT, silt particle content; RA, relief amplitude; RU, roughness; SLO, slope; RHU, first principal component value of principal component analysis of mean relative humidity in autumn and spring; EVI, enhanced vegetation index; ATEMWI, accumulated temperature in winter; SOC, soil organic carbon content; STN, soil total nitrogen content.

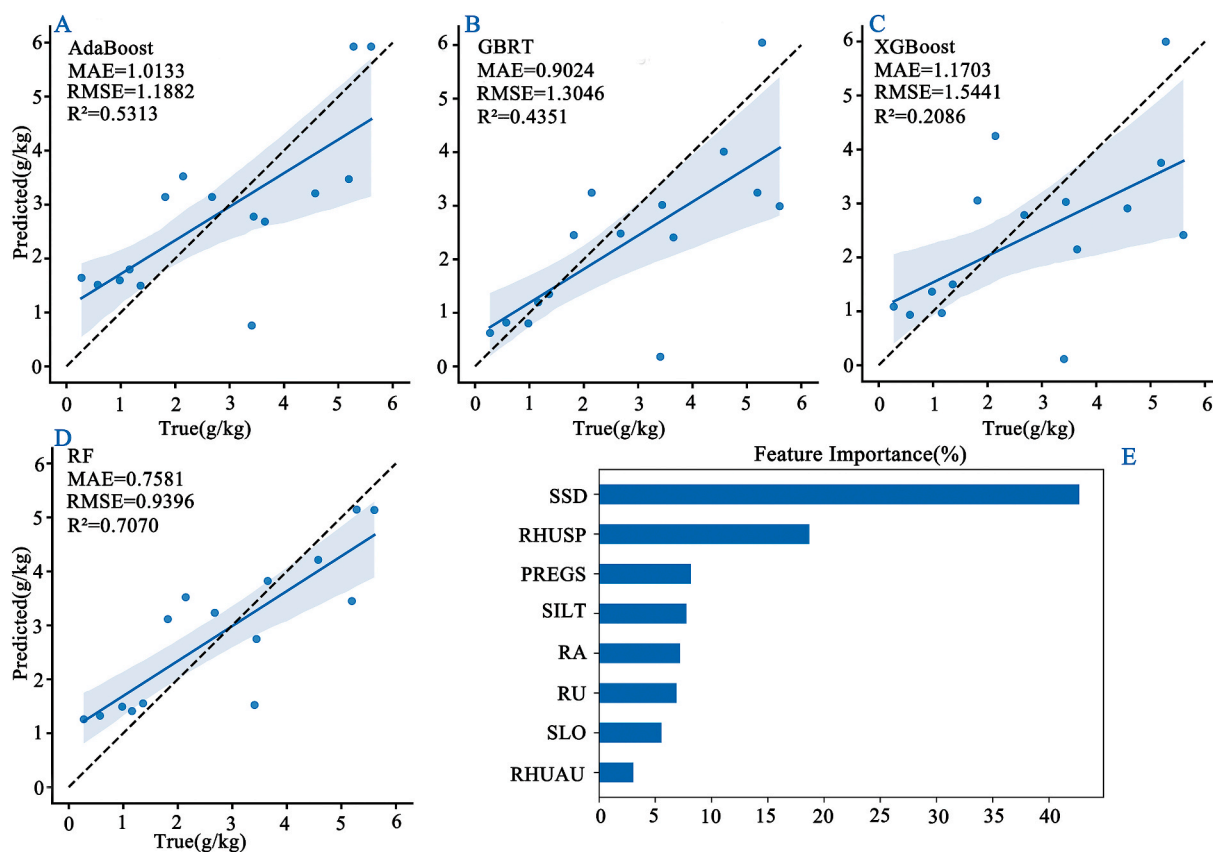


**Fig. 3.** Predicted vs. True SOC of validation dataset derived from (A) Adaptive Boosting Regressor (AdaBoost), (B) Gradient Boosting Regression (GBRT), (C) Extreme gradient boosting Regression (XGBoost), (D) Random Forest Regression (RF), (E) variables of importance for RF (SSD = Annual sunshine duration, RHUSP = Mean relative humidity in spring, PREGS=Precipitation in growing season, SILT=Silt particle content, RA = Relief Amplitude, RU = Roughness, SLO=Slope, RHUAU = Mean relative humidity in autumn).

one of the main drivers affecting SOC and STN of arid and semi-arid regions. By analysing data from meteorological stations in the study area from 2000 to 2019, we found that there was no obvious variation trend in ATEMWI, PREGS increased trend at a rate of 12.9mm/decade and average was 119.85 mm, and eight years were above average (Fig. 5 left). The average RHUSP and RHUAU were 30.90% and 47.91%, respectively, showing a decreasing trend with ratios of  $-1.2\%/decade$

and  $-2.0\%/decade$  (Fig. 5 middle). It showed that relative humidity was higher in autumn than in spring, however, the rate of decline was higher in autumn than in spring. Moreover, the average SSD was 3117.10h and had a significant decreasing trend of 60 h/decade (Fig. 5 right). Among many meteorological elements, SSD changed significantly and with the highest slope of change (Fig. 5).

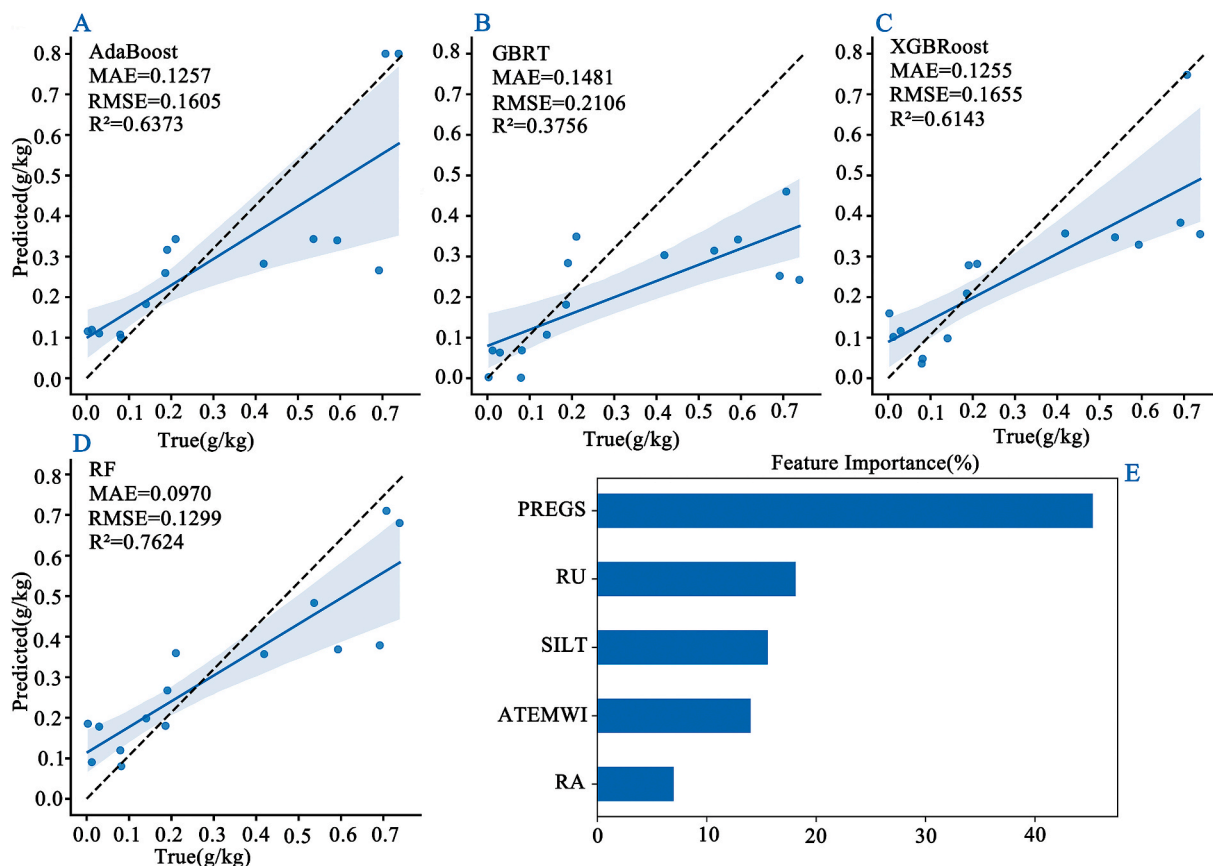


Fig. 4. Predicted vs. True STN of validation dataset derived from (A) Adaptive Boosting Regressor (AdaBoost), (B) Gradient Boosting Regression (GBRT), (C) Extreme gradient boosting Regression (XGBRoost), (D) Random Forest Regression (RF). (E) variables of importance for RF (PREGS=Precipitation in growing season, RU = Roughness, SILT=Silt particle content, ATEMWI = Accumulated temperature in winter, RA = Relief Amplitude).

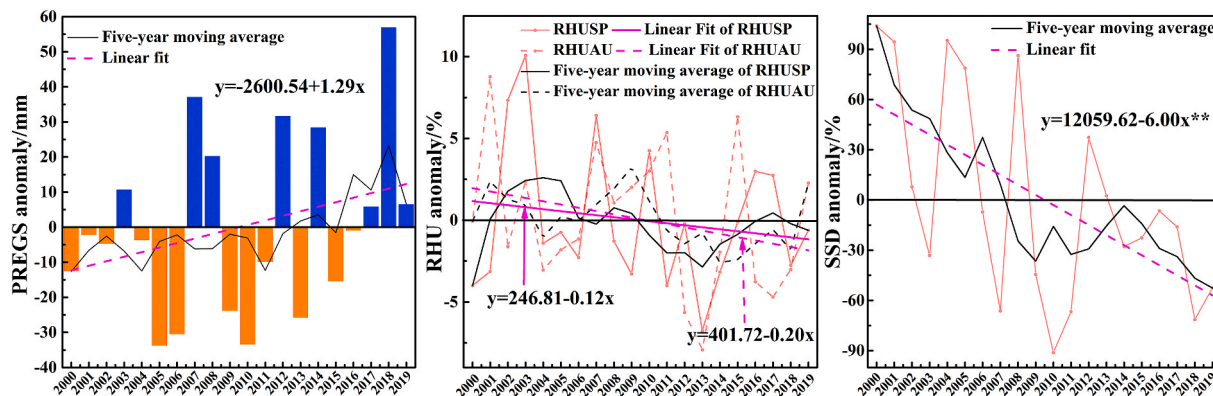


Fig. 5. Meteorological element anomaly map of the study area from 2000 to 2019. Y = 0 represents the average value from 2000 to 2019. The value above this line means greater than average value and below this line means less than average value.

### 3.5. Effects of climate change on SOC and STN

Overall, RF accurately predicted SOC and STN, while climate was the most important driver affecting SOC and STN. From 2000 to 2019, the meteorological elements (PREGS, RHUSP, RHUAU, and SSD) in the study area showed different trends, but how did they affect the SOC and STN? In contrast to the relatively stable topographic elements and soil texture in the short term (<20 years), the changes in meteorological elements were more sensitive. This study assumes that RA, RU, SLO, and SILT were unchanged from 2000 to 2019 and has explored the effects of climate change on the SOC, STN and SOC/STN. Finally, we used climate

variables data collected from the sampling sites from 2000 to 2019 and combined it with the prediction model established in Section 3.3 to predict SOC and STN from 2000 to 2019. Results showed that in dryland, climate change increased SOC at a rate of 0.04 g/kg/decade, decreased STN at a rate of 0.003 g/kg/decade, and increased SOC/STN at a ratio of 1.1/decade, unsteadily (Fig. 6). In the context of climate change, dryland was a potential source of carbon sequestration, but it was unstable. It changed dynamically from year to year because of the annual hydrothermal variance tendency, leading to STN loss, which reduced soil fertility. More attention should be paid to STN monitoring in dryland in the future.

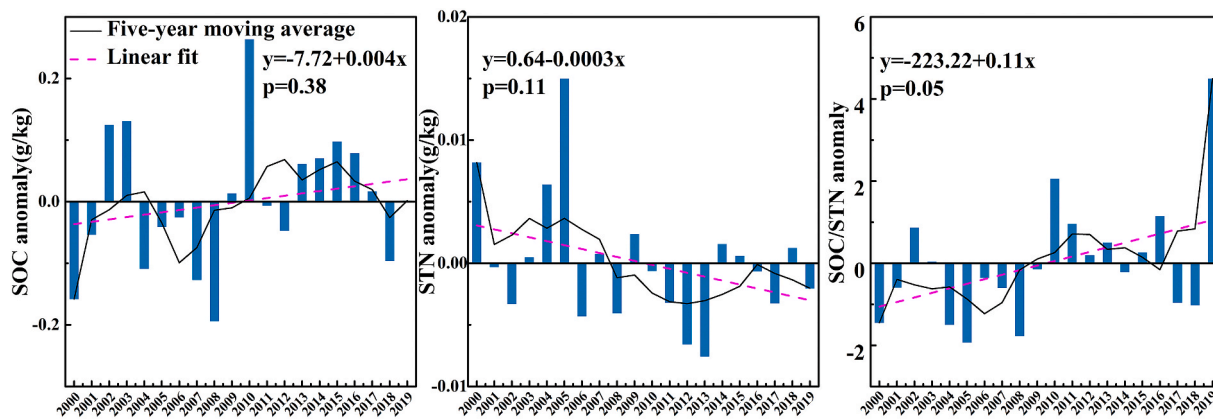


Fig. 6. Change trend of SOC, STN and SOC/STN from 2000 to 2019.  $Y = 0$  represents the average value from 2000 to 2019. The value above the line means greater than average value, and below the line is less than average.

## 4. Discussion

### 4.1. Effects factors on SOC and STN in dryland

Both the RF model (Figs. 2 and 3) and the SEM (Fig. 4 and Table 2) model all showed that climate elements were the most influential predictor variables in dryland to predict SOC and STN. It was different from mountain and farmland ecosystems, where other factors such as topography and soil type were the main influencing factors (Zhu et al., 2010; Iqbal et al., 2005). Due to the low soil fertility of dryland, these areas are exceedingly sensitive to degradation caused by climate change (Li et al., 2016). Climate is closely related to SOC and STN input and decomposition, such as affecting vegetation distribution and growth and restricting litter decomposition (Li et al., 2020). For example, temperature can lead to the dissociation of soil element stoichiometry and microbial activity (Mooshammer et al., 2017). Precipitation has an implication in nutrient cycling, and is related to leaching intensity (Gordon et al., 2008), which directly affects SOC and STN; meanwhile, it also affects plant growth and indirectly affects SOC and STN (Tang et al., 2019). Different from other ecosystems, photodegradation is the main governing factor of surface litter decomposition in dryland ecosystems (Moorhead and Callaghan, 1994). It may explain why most of the carbon fixed by plants is directly lost to the atmosphere instead of contributing to soil organic matter (Austin and Vivanco, 2006). However, in the study area, the dramatic SSD decline from 2000 to 2019 would weaken the photodegradation potential due to the increased precipitation in the growing season (Austin and Vivanco, 2006). In addition, the change in precipitation was correlated with higher and lower RHU (Elliott and Angell, 1997; Kawamoto, 2006). Topography controls the flow of solutes, water, and sediments, affecting soil development and spatial distribution of soil nutrients (Li et al., 2013). Some topographic features have been proven to have a highly significant correlation (e.g., RA, RU, and SLO) with SOC and STN (Wang et al., 2017), but they indirectly affect SOC and STN by affecting soil texture that affects SOC and STN because silt and clay particles provide physical protections of SOC and STN and promote its aggregation (Zinn et al., 2005).

In previous studies, when meteorological elements were used to predict SOC and STN, the focus was on the annual statistical value of meteorological elements (Li et al., 2020; Mahmoudzadeh et al., 2020), while their seasonal statistical values were ignored. However, increasing evidence shows seasonal changes in meteorological elements affect vegetation growth, thus affecting SOC and STN. The accumulated temperature in spring will affect the spring phenology and the time of frost (Yu et al., 2010). Stabilisation of carbon sequestration in a Chinese desert steppe benefits from increased temperatures and precipitation outside the growing season (Yang et al., 2019). Summer precipitation was important for autumn vegetation growth in the arid region, where

summer temperature increased autumn vegetation growth in semi-arid and semi-humid regions (Wang et al., 2021; Xie et al., 2016). Cumulative precipitation during the growing season had a dominant effect on the vegetation dynamics compared with temperature for some vegetation types (Liu et al., 2015). The above conclusion was consistent with the results of this study. Seasonal statistical values of meteorological elements (PREGS, RHUSP, RHUAU, and ATEMWI) will affect the growth of vegetation, thus affecting SOC and STN.

### 4.2. Performance of predictive models in dryland

The comparative prediction accuracy in this study showed that the RF model well predicted SOC and STN in drylands compared to the other three prediction models (Figs. 2 and 3). This result is consistent with Zeraatpisheh et al. (2019), who proved that RF had the highest performance to predict SOC in dryland, central Iran. The main reason is that an RF model could use the regression model in the terminal nodes to produce a series of predictions with the prominent ability of RF as its prediction capacity (Prasad et al., 2006). Of course, as predicting SOC and STN based on soil-landscape model, though different machine learning algorithms perform differently in various landscape types, RF often showed excellent performance, such as humid tropical and subtropical regions (Keskin et al., 2019) and dry and half-dry regions (Mahmoudzadeh et al., 2020). Even in some areas, the accuracy is not as high as other methods, but the differences are small. For example, Zhou et al. (2020) showed that the boosted regression trees (BRT) model outperformed the RF model (SOC:  $R^2 = 0.44$  vs  $R^2 = 0.40$ , STN:  $R^2 = 0.38$  vs  $R^2 = 0.38$ ) in the southern region of Central Europe, where forests and ploughland are the main land-use types, but the discrepancy was small. Khanal et al. (2018) showed that in an area where farmland is the main land-use type, the neural network model provided the highest accuracy compared to RF, but the discrepancy was also small ( $R^2 = 0.60$  vs  $R^2 = 0.54$ ). Overall, the RF algorithm may be the most appropriate model when using the soil-landscape model to predict SOC and STN in arid and semi-arid areas.

### 4.3. Effect of interannual hydrothermal variability on SOC and STN in dryland

In dryland, climate change increases C sequestration (Fig. 6). The result was consistent with the conclusions of many researchers. A previous study showed that the desert steppe ecosystem was a net C source because of high temperatures and drought (Zeng et al., 2005), but this may be counteracted by climate change effects which can prolong the growing season and increase C sink (Wang et al., 2018a). Other research found the desert steppe was a weak C sequestration whether combined carbon stocks with regional models or a soil nutrient cycling model with

C flux measurements at a local scale (Wu et al., 2018; Yang et al., 2019). The decrease of SSD in the study area from 2000 to 2019 may weaken photodegradation and accelerate more carbon flowing into the soil carbon pool, causing an increase in SOC (Austin and Vivanco, 2006). PREGS increase usually enhances ecosystem C gain by increasing biomass (She et al., 2016). However, STN showed an opposite trend, and climate change would lead to the loss of STN (Fig. 6). N transformation in soil is often controlled by soil temperature, moisture, soil texture, and pH (Burke, 1989; Zhou et al., 2020). Precipitation will change the temporal patterns of N cycling due to the sensitivity of different N transform to soil moisture (Fierer and Schimel, 2002; Ladwig et al., 2015), denitrification and the production of N<sub>2</sub>O increases with increasing soil moisture (Hu et al., 2015). NO<sub>3</sub>-N can be significantly high in drained or seasonally dry areas (Hanlon et al., 1997), and NO<sub>3</sub>-N is usually more leachable due to its negative charge (Liao et al., 2016). Therefore, under climate change, the increase of precipitation in the growing season strengthened soil leaching and denitrification, eventually decreasing total N concentration. Moreover, C and N cycles in terrestrial ecosystems are two processes that are closely related to each other. Climate change would prolong the growing season of plants, stimulate photosynthesis, increase plant biomass, and enhance ecosystem C gains (Luo et al., 2009). However, C fixation was regulated by the availability of N by plants, and the increase of carbon fixation of the plant was bound to increase nitrogen acquisition in soil. In the future, N limitation in dryland ecosystems will be more and more serious in the context of climate change.

## 5. Conclusion

Overall, in dryland, the RF model performed better in predicting SOC and STN than the other three prediction models (AdaBoost, GBRT, XGBoost). In the future, we can use the method to investigate SOC and STN in arid areas with less population and poor roads. Climate factors were the main factors affecting SOC and STN in the study area; SOC and STN can be preliminarily diagnosed by monitoring the change of meteorological elements. In Alashan area, a dryland in northern China, the precipitation in the growing season showed an increasing trend from 2000 to 2019, at a rate of 12.9mm/decade. During the same period, the annual sunshine duration significantly decreased by 66 h/decade. In study areas, climate change increased SOC at a rate of 0.04 g/kg/decade and decreased STN by 0.003 g/kg/decade from 2000 to 2019 at an unstable rate. In the context of climate change, dryland was a potential site for carbon sequestration, but it is unstable. It changes dynamically yearly because of annual hydrothermal variability, resulting in loss of STN and ultimately reducing soil fertility. More attention should be paid to STN monitoring in dryland in the future.

## Author contributions

Mingzhu He and Liang Tang: Data curation, building the model, writing and revising the manuscript, methodology. Chengyi Li, Jianxin Ren, Libin Zhang, Manfei Li: Technical assistance, data curation, participation in discussions.

## Declaration of competing interest

The authors declare that they have no known competing financial interests or personal relationships that could have appeared to influence the work reported in this paper.

The authors declare no conflicts of interest.

## Acknowledgements

This study was supported by the Strategic Priority Research Program of Chinese Academy of Sciences (No. XDA 2003010301), National Natural Science Foundation of China (No. 41671103), and Research and

Development Funds of Transport Bureau of Ningxia Hui Autonomous Region (WMKY1).

## References

- Albataineh, A.S., 2019. A gradient boosting regression based approach for energy consumption prediction in buildings. *Adv. Energy Res.* 6 (2), 91–101.
- Austin, A.T., Vivanco, L., 2006. Plant litter decomposition in a semi-arid ecosystem controlled by photodegradation. *Nature* 442 (7102), 555–558.
- Avnimelech, R., Intrator, N., 1999. Boosting regression estimators. *Neural Comput.* 11 (2), 499–520.
- Bai, W.M., Wan, S.Q., Niu, S.L., Liu, W.X., Chen, Q.S., Wang, Q.B., Zhang, W.H., Han, X.G., Li, L.H., 2010. Increased temperature and precipitation interact to affect root production, mortality, and turnover in a temperate steppe: implications for ecosystem C cycling. *Global Change Biol.* 16 (4), 1306–1316.
- Bonatti, E.E., Decant, J.P., Munson, S.M., Gathany, M.A., Przeszlowska, A., Haddix, M.L., Owens, S., Burke, I.C., Parton, W.J., Harmon, M.E., 2009. Litter decomposition in grasslands of central north America (US great plains). *Global Change Biol.* 15 (5), 1356–1363.
- Breiman, L., 2001. Random forests. *Mach. Learn.* 45 (1), 5–32.
- Burke, I.C., 1989. Control of nitrogen mineralization in a sagebrush steppe landscape. *Ecology* 70 (4), 1115–1126.
- Chen, T.Q., Guestrin, C., 2016. XGBoost: a scalable tree boosting System. In: *Proceedings of the 22nd acm sigkdd international conference on knowledge discovery and data mining*. KDD, San Francisco, CA, pp. 785–794.
- Elliott, W.P., Angell, J.K., 1997. Variations of cloudiness, precipitable water, and relative humidity over the United States: 1973–1993. *Geophys. Res. Lett.* 24 (1), 41–44.
- Fang, X., Guo, X.L., Zhang, C., Shao, H., Zhu, S.H., Li, Z.Q., Feng, X.W., He, B., 2019. Contributions of climate change to the terrestrial carbon stock of the arid region of China: a multi-dataset analysis. *Sci. Total Environ.* 668, 631–644.
- Fierer, N., Schimel, J.P., 2002. Effects of drying–rewetting frequency on soil carbon and nitrogen transformations. *Soil Biol. Biochem.* 34 (6), 777–787.
- Forkuor, G., Hounkpatin, O.K.L., Welp, G., Thiel, M., 2017. High resolution mapping of soil properties using remote sensing variables in south-western Burkina Faso: a comparison of machine learning and multiple linear regression models. *PLoS One* 12 (1), e0170478.
- Friedman, J.H., 2001. Greedy function approximation: a gradient boosting machine. *Ann. Stat.* 29 (5), 1189–1232.
- Gholizadeh, A., Zizala, D., Saberioon, M., Boruvka, L., 2018. Soil organic carbon and texture retrieving and mapping using proximal, airborne and Sentinel-2 spectral imaging. *Remote Sens. Environ.* 218, 89–103.
- Gordon, H., Haygarth, P.M., Bardgett, R.D., 2008. Drying and rewetting effects on soil microbial community composition and nutrient leaching. *Soil Biol. Biochem.* 40 (2), 302–311.
- Grace, J., San Jose, J., Meir, P., Miranda, H.S., Montes, R.A., 2006. Productivity and carbon fluxes of tropical savannas. *J. Biogeogr.* 33 (3), 387–400.
- Grace, J.B., Keeley, J.E., 2006. A structural equation model analysis of postfire plant diversity in California shrublands. *Ecol. Appl.* 16 (2), 503–514.
- Guo, S.X., Zhu, A.X., Meng, L.K., Burt, J.E., Du, F., Liu, J., Zhang, G.M., 2016. Unification of soil feedback patterns under different evaporation conditions to improve soil differentiation over flat area. *Int. J. Appl. Earth Obs. Geoinf.* 49, 126–137.
- Hanlon, E.A., Anderson, D.L., Diaz, O.A., 1997. Nitrogen mineralization in histosols of the everglades agricultural area. *Commun. Soil Sci. Plant Anal.* 28 (1–2), 73–87.
- Hartmann, A.A., Barnard, R.L., Marhan, S., Niklaus, P.A., 2013. Effects of drought and N-fertilization on N cycling in two grassland soils. *Oecologia* 171 (3), 705–717.
- Holz, M., Zarebanadkouki, M., Kaestner, A., Kuzuyakov, Y., Carminati, A., 2018. Rhizodeposition under drought is controlled by root growth rate and rhizosphere water content. *Plant Soil* 423 (1–2), 429–442.
- Hu, J., Inglett, K.S., Clark, M.W., Inglett, P.W., Reddy, K.R., 2015. Nitrous oxide production and consumption by denitrification in a grassland: effects of grazing and hydrology. *Sci. Total Environ.* 532, 702–710.
- Huang, J.P., Yu, H.P., Dai, A.G., Wei, Y., Kang, L.T., 2017. Drylands face potential threat under 2 degrees C global warming target. *Nat. Clim. Change* 7 (6), 417–422.
- Huete, A., Didan, K., Miura, T., Rodriguez, E.P., Gao, X., Ferreira, L.G., 2002. Overview of the radiometric and biophysical performance of the MODIS vegetation indices. *Remote Sens. Environ.* 83 (1–2), 195–213.
- Iqbal, J., Thomasson, J.A., Jenkins, J.N., Owens, P.R., Whisler, F.D., 2005. Spatial variability analysis of soil physical properties of alluvial soils. *Soil Sci. Soc. Am. J.* 69 (4), 1338–1350.
- Kalambukattu, J.G., Kumar, S., Raj, R.A., 2018. Digital soil mapping in a Himalayan watershed using remote sensing and terrain parameters employing artificial neural network model. *Environ. Earth. Sci.* 77 (5), 203.
- Kawamoto, K., 2006. Relationships between cloud properties and precipitation amount over the Amazon basin. *Atmos. Res.* 82 (1–2), 239–247.
- Keskin, H., Grunwald, S., Harris, W.G., 2019. Digital mapping of soil carbon fractions with machine learning. *Geoderma* 339, 40–58.
- Khanal, S., Fulton, J., Klopfenstein, A., Douridas, N., Shearer, S., 2018. Integration of high resolution remotely sensed data and machine learning techniques for spatial prediction of soil properties and corn yield. *Comput. Electron. Agric.* 153, 213–225.
- Ladwig, L.M., Sinsabaugh, R.L., Collins, S.L., Thomey, M.L., 2015. Soil enzyme responses to varying rainfall regimes in Chihuahuan Desert soils. *Ecosphere* 6 (3), 40.
- Leiningen, W.G.Z., 1931. Dokuchaiev's ideas in the development of pedology and cognate sciences. *Petermanns Mitt* 77 (7–8), 209–209.
- Li, B.F., Chen, Y.N., Shi, X., 2012. Why does the temperature rise faster in the arid region of northwest China? *J. Geophys. Res. Atmos.* 117, D16115.

- Li, J.W., Liu, Z.F., He, C.Y., Tu, W., Sun, Z.X., 2016. Are the drylands in northern China sustainable? A perspective from ecological footprint dynamics from 1990 to 2010. *Sci. Total Environ.* 553, 223–231.
- Li, Q.-q., Yue, T.X., Wang, C.Q., Zhang, W.J., Yu, Y., Li, B., Yang, J., Bai, G.C., 2013. Spatially distributed modeling of soil organic matter across China: an application of artificial neural network approach. *Catena* 104, 210–218.
- Li, Y., Ma, J., Xiao, C., Li, Y., 2020. Effects of climate factors and soil properties on soil nutrients and elemental stoichiometry across the Huang-Huai-Hai River Basin, China. *J. Soils Sediments* 20 (4), 1970–1982.
- Liao, X., Inglett, P.W., Inglett, K.S., 2016. Seasonal patterns of nitrogen cycling in subtropical short-hydroperiod wetlands: effects of precipitation and restoration. *Sci. Total Environ.* 556, 136–145.
- Liu, X., Zhu, X., Li, S., Liu, Y., Pan, Y., 2015. Changes in growing season vegetation and their associated driving forces in China during 2001–2012. *Rem. Sens.* 7 (11), 15517–15535.
- Liu, Y.J., Chen, J., 2021. Future global socioeconomic risk to droughts based on estimates of hazard, exposure, and vulnerability in a changing climate. *Sci. Total Environ.* 751, 142159.
- Luo, Y.Q., Sherry, R., Zhou, X.H., Wan, S.Q., 2009. Terrestrial carbon-cycle feedback to climate warming: experimental evidence on plant regulation and impacts of biofuel feedstock harvest. *Global Change Biol.* 1 (1), 62–74.
- Mahmoudzadeh, H., Matinfar, H.R., Taghizadeh-Mehrjardi, R., Kerry, R., 2020. Spatial prediction of soil organic carbon using machine learning techniques in western Iran. *Geoderma Reg* 21, e00260.
- Mikha, M.M., Rice, C.W., Milliken, G.A., 2005. Carbon and nitrogen mineralization as affected by drying and wetting cycles. *Soil Biol. Biochem.* 37 (2), 339–347.
- Moorhead, D.L., Callaghan, T., 1994. Effects of increasing ultraviolet-B radiation on decomposition and soil organic-matter dynamics - A synthesis and modeling study. *Biol. Fertil. Soils* 18 (1), 19–26.
- Mooshammer, M., Hofhansl, F., Frank, A.H., Wanek, W., Haemmerle, I., Leitner, S., Schneckler, J., Wild, B., Watzka, M., Keiblinger, K.M., Zechmeister-Boltenstern, S., Richter, A., 2017. Decoupling of microbial carbon, nitrogen, and phosphorus cycling in response to extreme temperature events. *Sci. Adv.* 3 (5), e1602781.
- Natekin, A., Knoll, A., 2013. Gradient boosting machines, a tutorial. *Front. Neurobot.* 7, 21.
- Prasad, A.M., Iverson, L.R., Liaw, A., 2006. Newer classification and regression tree techniques: bagging and random forests for ecological prediction. *Ecosystems* 9 (2), 181–199.
- Ren, C.J., Zhao, F.Z., Shi, Z., Chen, J., Han, X.H., Yang, G.H., Feng, Y.Z., Ren, G.X., 2017. Differential responses of soil microbial biomass and carbon-degrading enzyme activities to altered precipitation. *Soil Biol. Biochem.* 115, 1–10.
- Reynolds, J.F., Stafford Smith, D.M., Lambin, E.F., Turner, B.L., Mortimore, M., Batterbury, S.P.J., Downing, T.E., Dowlatabadi, H., Fernandez, R.J., Herrick, J.E., Huber-Sannwald, E., Jiang, H., Leemans, R., Lynam, T., Maestre, F.T., Ayarza, M., Walker, B., 2007. Global desertification: building a science for dryland development. *Science* 316 (5826), 847–851.
- Scornet, E., Biau, G., Vert, J.P., 2015. Consistency of random of random forest. *Ann. Stat.* 43 (4), 1716–1741.
- Seo, D.K., Kim, Y.H., Eo, Y.D., Park, W.Y., Park, H.C., 2017. Generation of radiometric, phenological normalized image based on random forest regression for change detection. *Rem. Sens.* 9 (11), 1163.
- Shahhosseini, M., Martinez-Feria, R.A., Hui, G.P., Archontoulis, S.V., 2019. Maize yield and nitrate loss prediction with machine learning algorithms. *Environ. Res. Lett.* 14 (12), 124026.
- She, W.W., Zhang, Y.Q., Qin, S.G., Wu, B., Bai, Y.X., 2016. Increased precipitation and nitrogen alter shrub architecture in a desert shrubland: implications for primary production. *Front. Plant Sci.* 7, 1908.
- Tajik, S., Ayoubi, S., Zeraatpisheh, M., 2020. Digital mapping of soil organic carbon using ensemble learning model in Mollisols of Hyrcanian forests, northern Iran. *Geoderma Reg.* 20, e00256.
- Tang, F.H.M., Riley, W.J., Maggi, F., 2019. Hourly and daily rainfall intensification causes opposing effects on C and N emissions, storage, and leaching in dry and wet grasslands. *Biogeochemistry* 144 (2), 197–214.
- Tanak, J.S., 1990. Structural equations with latent - variables - bollen, KA. *Appl. Psychol. Meas.* 14 (2), 213–215.
- Ullman, J.B., 2001. A first course in structural equation modeling. *Appl. Psychol. Meas.* 25 (1), 101–102.
- Walkley, A., Black, I.A., 1934. An examination of the Degtjareff method for determining soil organic matter, and a proposed modification of the chromic acid titration method. *Soil Sci.* 37 (1), 29–38.
- Wang, C.Y., Yu, M.H., Ding, G.D., Gao, G.L., Zhang, L.L., 2021. Effect of rainfall on *Artemisia ordosica* Krasch annual net primary production and allocation in sandy land in China. *Ecol. Indic.* 130, 108023.
- Wang, L., Tian, F., Wang, Y., Wu, Z., Schurgers, G., Fensholt, R., 2018a. Acceleration of global vegetation greenup from combined effects of climate change and human land management. *Global Change Biol.* 24 (11), 5484–5499.
- Wang, S., Adhikari, K., Wang, Q., Jin, X., Li, H., 2018b. Role of environmental variables in the spatial distribution of soil carbon (C), nitrogen (N), and C:N ratio from the northeastern coastal agroecosystems in China. *Ecol. Indic.* 84, 263–272.
- Wang, S., Zhuang, Q., Wang, Q., Jin, X., Han, C., 2017. Mapping stocks of soil organic carbon and soil total nitrogen in Liaoning Province of China. *Geoderma* 305, 250–263.
- Wieder, W.R., Cleveland, C.C., Smith, W.K., Todd-Brown, K., 2015. Future productivity and carbon storage limited by terrestrial nutrient availability. *Nat. Geosci.* 8 (6), 441–444.
- Wright, S., 1934. The method of path coefficients. *Ann. Math. Stat.* 5, 161–215.
- Wu, X., Kang, X.M., Liu, W.J., Cui, X.Y., Hao, Y.B., Wang, Y.F., 2018. Using the DNDC model to simulate the potential of carbon budget in the meadow and desert steppes in Inner Mongolia, China. *J. Soils Sediments* 18 (1), 63–75.
- Xie, B., Jia, X., Qin, Z., Shen, J., Chang, Q., 2016. Vegetation dynamics and climate change on the Loess Plateau, China: 1982–2011. *Reg. Environ. Change* 16 (6), 1583–1594.
- Yang, B., Gong, J., Zhang, Z., Wang, B., Zhu, C., Shi, J., Liu, M., Liu, Y., Li, X., 2019. Stabilization of carbon sequestration in a Chinese desert steppe benefits from increased temperatures and from precipitation outside the growing season. *Sci. Total Environ.* 691, 263–277.
- Yu, H.Y., Luedeling, E., Xu, J.C., 2010. Winter and spring warming result in delayed spring phenology on the Tibetan Plateau. *P. Natl. Acad. Sci. USA.* 107 (51), 22151–22156.
- Yuan, S., Fu, H.P., Wu, X.D., Yang, S.W., Malqin, X.G., Yue, X.X., 2018. Effects of grazing on the northern three-toed jerboa pre- and post-hibernation. *J. Wildl. Manag.* 82 (8), 1588–1597.
- Zeng, N., Qian, H.F., Roedenbeck, C., Heimann, M., 2005. Impact of 1998–2002 midlatitude drought and warming on terrestrial ecosystem and the global carbon cycle. *Geophys. Res. Lett.* 32 (22), L22709.
- Zeraatpisheh, M., Ayoubi, S., Jafari, A., Tajik, S., Finke, P., 2019. Digital mapping of soil properties using multiple machine learning in a semi-arid region, central Iran. *Geoderma* 338, 445–452.
- Zhou, T., Geng, Y.J., Chen, J., Pan, J.J., Haase, D., Lausch, A., 2020. High-resolution digital mapping of soil organic carbon and soil total nitrogen using DEM derivatives, Sentinel-1 and Sentinel-2 data based on machine learning algorithms. *Sci. Total Environ.* 729, 138244.
- Zhu, A.X., Liu, F., Li, B.L., Pei, T., Qin, C.Z., Liu, G.H., Wang, Y.J., Chen, Y.N., Ma, X.W., Qi, F., Zhou, C.H., 2010. Differentiation of soil conditions over low relief areas using feedback dynamic patterns. *Soil Sci. Soc. Am. J.* 74 (3), 861–869.
- Zinn, Y.L., Lal, R., Resck, D.V.S., 2005. Texture and organic carbon relations described by a profile pedotransfer function for Brazilian Cerrado soils. *Geoderma* 127 (1–2), 168–173.